Towards the calibration of terrestrial laser scanners – A case study at a water dam

Eike KOLLER[1,*], **Berit JOST**[1], and **Heiner KUHLMANN**[1]

[1] *Institute of Geodesy and Geoinformation, University of Bonn, Germany, (e.koller@igg.uni-bonn.de)*

[*] *corresponding author*

Abstract

Internal misalignments in terrestrial laser scanners (TLS) lead to systematic errors in the magnitude of certain millimeters in their point clouds. For deformation analyses with high accuracy requirements, these geometric imperfections must be determined to correct the point cloud by calibration. Neglecting proper calibrations can result in misinterpretations during the deformation analysis, as any systematic errors may be interpreted as deformation. The manufacturers calibrate the scanners before delivery. Due to aging processes of the scanners and external influences such as temperature, geometric imperfections change over time and recalibration becomes necessary. This also limits the utility of installed calibration fields for a-priori calibrations. In this study, we demonstrate a way to calibrate a panoramic-type TLS during a measurement (in-situ) using a concrete water dam. Point clouds of the dam from several stations are used to estimate calibration parameters. The parameters are determined by artificial targets placed in the environment and via distinctive points in the point cloud itself. The study provides a procedure to estimate calibration parameters at a concrete water dam. It can be shown that a calibration reduces systematic effects in TLS point clouds. This minimizes the risk of misinterpreting systematic errors as deformations.

Keywords: terrestrial laser scanner, calibration, quality assurance

1 Introduction

Terrestrial laser scanners (TLS) have become a standard tool in engineering geodesy due to their capability for large-scale area measurements and surface capturing. Beyond applications with lower accuracy demands, TLS are also employed for deformation monitoring, where data quality is critical.

In addition to random measurement noise, various systematic effects can occur, including errors caused by internal misalignments in TLS. For instance, constructional imperfections or internal mechanical changes due to temperature, aging, etc. can introduce systematic errors in point clouds (Muralikrishnan, 2021), which may be misinterpreted as deformations for example in monitoring applications. To mitigate these effects, TLS calibration is essential, allowing systematic errors to be identified and mathematically corrected in the point cloud. Different functional models describe the impact of mechanical misalignments on the observation depending on calibration parameters (CPs) (Wang et al., 2017; Lichti, 2007). The task of TLS calibration is to determine these parameters.

For high-precision applications, regular determination of the CPs is essential to maintain accuracy. Since these parameters are unstable and vary over different time scales (Medić et al., 2021), a one-time calibration by the manufacturer before delivery is insufficient. While manufacturers offer recalibration services, users also have the option to determine and apply calibration values independently. These values can be obtained either before measurement (a-priori) or during measurement (in-situ).

Several studies have developed calibration strategies and optimized calibration fields (e.g. Lichti et al. (2021); Medić et al. (2019b)) to determine the CPs a-priori, thereby enhancing point cloud quality. However, for these approaches to be successful, certain prerequisites must be met: By using classical TLS targets to determine CPs, a sufficient number of targets must be available, or an optimized measurement geometry must be ensured (Medić et al., 2019b). However, meeting these requirements may sometimes be impractical, especially if access to a permanently installed calibration field is not possi-

ble. Additionally, calibration should be conducted as close as possible to the actual measurement in both time and location. To address this issue, an in-situ calibration can be particularly useful. In this case, data that is already being captured can be leveraged to derive the CPs.
In this study, we develop and examine two approaches for implementing in-situ calibration on water dams. We focus on panoramic TLS:

- We use Two-Face Method to determine CPs from a single station by comparing front and back face measurement using keypoints extracted from the point cloud.
- We enhance the functional model of Two-Face Method and adding artificial targets in the environment we include the Network Method to achrive a combined method. CPs are estimated via a registration process.

The Two-Face Method from one single station allows only to estimate a subset of CPs, while the combined approach allows to estimate all of them.
As critical infrastructure, dams require regular deformation monitoring to prevent potential failures and associated risks and catastrophes. TLS are well-suited for this task, as it enables rapid data acquisition and area-based analyses. However, without proper calibration, ensuring the quality and reliability of the collected data is not possible.
Chapter 2 provides an overview of the theoretical background of TLS calibration and outlines various approaches for determining CPs. In Chapter 3 we describe a measurement setup that enables to apply described approaches, while chapter 4 presents calibration results. We discuss these results in chapter 5 and finally, chapter 6 concludes the presented work.

2 Material and Methods

In this study, we employ self-calibration methods, which offer the advantage of not requiring external reference length of coordinates. Instead, calibration relies solely on identical targets that are visible in front and back face scans and potentially from different stations. These targets can be signalized using artificial TLS targets or identified through keypoints. These keypoints must be extracted from the point clouds and matched to their corresponding counterparts across different scans. Typically, these keypoints are less accurate compared to artificial targets, but the number of these points is commonly much higher.

Table 1. Parameters of geometric error model developed by NIST. $(.)*$ indicates two-face sensitivity.

CP	Description
x_{1n}, $x_{1z}*$	hor.l/vert. beam offset
x_2*	hor. axis offset
x_3*	mirror offset
x_4*	vert. index offset
x_{5n}, $x_{5z}*$	hor./vert. beam offset
x_6*	mirror tilt
x_7*	hor. axis tilt
$x_{8x}*$,$x_{8y}*$	hor. angle encoder eccentricity
$x_{9n}*$,x_{9z}	vert. angle encoder eccentricity
x_{10}	rangefinder offset
x_{11a}, x_{11b}	2^{nd} order scale error (hor.)
$x_{12a}*$, x_{12b}	2^{nd} order scale error (ver.)

2.1 Impact of Calibration Parameters

TLS are polar measuring systems which measure a distance r_i^j, a horizontal angle φ_i^j and a vertical angle θ_i^j for each point i on station j. The cartesian coordinates can be expressed by spherical coordinate via (Schwarz, 2018)

$$\mathbf{X}_i^j = \begin{bmatrix} x_i^j \\ y_i^j \\ z_i^j \end{bmatrix} = \begin{bmatrix} r_i^j \cdot \sin\theta_i^j \cdot \cos\varphi_i^j \\ r_i^j \cdot \sin\theta_i^j \cdot \sin\varphi_i^j \\ r_i^j \cdot \cos\theta_i^j \end{bmatrix}. \quad (1)$$

We are using the geometric error model developed by the National Institute of Standards and Technology (NIST) (Wang et al., 2017). This model describes the functional impact of the mechanical misalignments by using a set of 18 CPs described in table 1. The table indicates that some CPs are two-face sensitive. Similar to total stations, resulting effects in front and back faces cancel each other out. The functional impacts on the spherical observations are shown in equations 2 - 4. Here, $k = 1$ for front face and $k = -1$ for back face measurement.

2.2 Two-Face Method

Most high-end laser scanners provide the capability to perform scans directly in two faces. Since nu-

$$\Delta r_i^j = k\left(x_2 \sin\theta_i^j) + x_{10}\right) \tag{2}$$

$$\Delta\varphi_i^j = k\left(\frac{x_{1z}}{r_i^j \tan\theta_i^j} + \frac{x_3}{r_i^j \sin\theta_i^j} + \frac{x_{5z}}{\tan\theta_i^j} + \frac{2x_6}{\sin\theta_i^j} - \frac{x_7}{\tan\theta_i^j} - x_{8x}\sin\varphi_i^j + x_{8y}\cos\varphi_i^j\right) + \frac{x_{1n}}{r_i^j} + x_{5n} + x_{11a}\cos 2\varphi_i^j + x_{11b}\sin 2\varphi_i^j \tag{3}$$

$$\Delta\theta_i^j = k\left(\frac{x_{1n}\cos\theta_i^j}{r_i^j} + \frac{x_2\cos\theta_i^j}{r_i^j} + x_4 + x_{5n}\cos\theta_i^j + x_{9n}\cos\theta_i^j\right) - \frac{x_{1z}\sin\theta_i^j}{r_i^j} - x_{5z}\sin\theta_i^j - x_{9z}\sin\theta_i^j + x_{12a}\cos 2\theta_i^j + x_{12b}\sin 2\theta_i^j \tag{4}$$

merous CPs from table 1 are sensitive to two faces, they can be determined by computing the difference of front and back face. This leads to the following functional model:

$$\mathbf{f}_i = \begin{bmatrix} x_i^f \\ y_i^f \\ x_i^f \end{bmatrix} - \begin{bmatrix} x_i^b \\ y_i^b \\ x_i^b \end{bmatrix} = \mathbf{0} \tag{5}$$

where $(.)^f$ indicate front and $(.)^b$ back face measurement. To integrate CPs as parameters into this model, we are using the spherical representation of a measured point by integrating the impact of CPs:

$$r_i^{f/b} = r_i^{f/b} + \Delta r_i^{f/b} \tag{6}$$

$$\varphi_i^{f/b} = \varphi_i^{f/b} + \Delta\varphi_i^{f/b} \tag{7}$$

$$\theta_i^{f/b} = \theta_i^{f/b} + \Delta\theta_i^{f/b}. \tag{8}$$

Equations 6-8 highlight the necessity of accessing spherical instead of cartesian observations. These can be derived by inverting equation 1. We estimate the CPs in a least squares adjustment by using an iterative Gauß-Helmert Model (Koch (2013)).

2.3 Combination of Two-Face and Network Method

We aim to enhance the Two-Face Method by integrating it with the Network Method, which estimates CPs as additional parameters in a registration process (for details see Reshetyuk (2009)). While both methods establish distinct functional relationships and could theoretically be applied in separate adjustments, we combine them into a global adjustment to jointly determine all CPs. Here we assume that measurements from both methods provide independent observations.

The algorithm for calculating CPs using the Network Method is based on a three-dimensional Helmert-Transform. Transformation parameters between a designated reference scan $\mathbf{X}^{ref}$ and at least one additional scan, which may originate from a different station or face is estimated by using

$$\mathbf{f}_i^j = \mathbf{R}^j\mathbf{X}^j + \mathbf{T}^j - \mathbf{X}^{ref} = \mathbf{0} \tag{9}$$

where $\mathbf{R}^j$ denotes the rotation matrix and $\mathbf{T}^j$ the translation vector. Analogous to the Two-Face Method, CPs are incorporated into the functional model by introducing their impact:

$$r_i^j = r_i^j + \Delta r_i^j \tag{10}$$

$$\varphi_i^j = \varphi_i^j + \Delta\varphi_i^j \tag{11}$$

$$\theta_i^j = \theta_i^j + \Delta\theta_i^j. \tag{12}$$

An iterative Gauss-Helmert model is employed to estimate the CPs (Koch, 2013). Additional parameters to be estimated are transformation parameters and the coordinates of the reference scan $\mathbf{X}^{ref}$. For more details see Reshetyuk (2009).

To combine Two-Face and Network Method, we summarize required vectors and matrices for both methods. As a result, the observation vector is given by $\bar{\mathbf{l}} = \begin{bmatrix}\mathbf{l}_{net}^T & \mathbf{l}_{2face}^T\end{bmatrix}^T$, the covariance matrix of observations by $\bar{\mathbf{C}}_{ll} = diag(\mathbf{C}_{ll_{net}}, \mathbf{C}_{ll_{2face}})$, the Design-matrix by $\bar{\mathbf{A}} = \begin{bmatrix}\mathbf{A}_{net}^T & \mathbf{A}_{2face}^T\end{bmatrix}^T$ and the condition matrix by $\bar{\mathbf{B}} = diag(\mathbf{B}_{net}, \mathbf{B}_{2face})$. Here, $(.)_{net}$ describes the parts of the Network Method and $(.)_{2face}$ of the Two-Face Method.

2.4 Feature Detection and Matching

The process of using keypoints instead of artificial targets involves two steps: first, salient points must be identified in all scans. This is achieved by detecting prominent points (often called features) using a *feature detector* and describing them with a *feature descriptor*. In the second step, feature matching is performed to associate identical points based on their feature descriptors. Various methods exist to carry out this process; however, we follow the approach outlined in Medić et al. (2019a), who developed an approach to estimate CPs using keypoints.
First, each point cloud j is represented as an intensity image and a range image. To achieve this, the points are converted into spherical coordinates. A regular grid is generated, where each grid cell corresponds to the measured horizontal angle φ_i^j along the horizontal axis and the vertical angle θ_i^j along the vertical axis. In the intensity image, we assign each grid cell with the measured intensity value, while in the range image, we assign each grid cell with the corresponding distance r_i^j.
To detect keypoints in the intensity image, we applied the Förstner operator (Förstner and Gülch, 1987), which allows for the identification of salient points at subpixel accuracy along with their associated covariance matrix. For feature description, we utilized the BRISK descriptor (Leutenegger et al., 2011), which serves as the basis for feature matching across all scans.
Each matched keypoint in the intensity image corresponds to a horizontal and vertical angle, which can be utilized for calibration. The covariance matrix of these angles is obtained through variance propagation from the covariance matrix computed by the Förstner operator for the detected keypoint. The corresponding distance for calibration is extracted from the range image. To enhance accuracy, we average all distances within a 5×5 pixel neighborhood around the keypoint. Outliers are filtered out using a Median Absolute Deviation (MAD) filter, and the variance of the averaged distances is used as the final distance variance.

3 Experimental Setup

In our experiments, we utilize a water dam with a crown length of about 200 m and a maximum height of approximately 25 m. Constructed from quarry stones, the dam has a correspondingly rough surface. Figure 1 provides an overview of the experimental setup. In total, we have placed 9 artificial TLS targets in the environment, T1 - T6 are located on the ground, T7-T9 on the crown. Except for target T7, BOTA8 targets were used (Janßen et al., 2019). In contrast, target T7 is a planar target designed for scanning from both sides. Scanners were positioned at stations S1-S3.

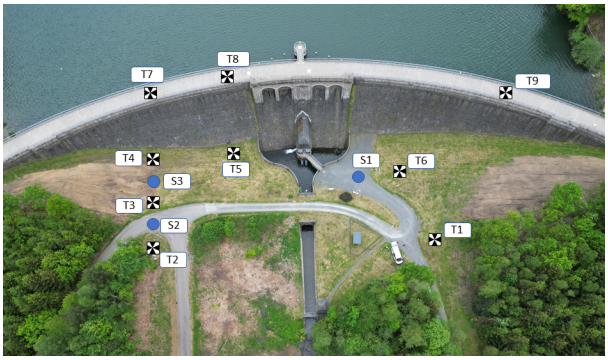

Figure 1. Overview of the experimental situation with target positions and used stations.

Station S1 is likely well suited for the Two-Face Method as it is positioned as close as possible to the dam. This station enables low vertical angles. This enhances the ability to determine CPs, as the impact of many mechanical misalignments is particularly large at low vertical angles (see equations 2- 3). Additionally, the change of faces of this station is chosen to be perpendicular to the dam, ensuring that both the front and back faces are captured within a single scan.
Stations 2 and 3 are well suited for the Network Method. The targets on the crown result in relatively small vertical angles, while there are sufficient targets in the horizon to determine CPs that are independent of the vertical angle. Distant targets in both the horizon and the zenith further improve the determination of the transformation parameters.
For data collection, we used the high-end TLS Z+F Imager5016. The dam was scanned with a spatial resolution of 3.1mm@10m and 1.6mm@10m. We have chosen the lowest quality settings in order to minimize the influence of the TLS software on the acquired data.
All scans were performed in front and back face. Lichti (2010) has shown that in the Network Method, correlations between the parameters are reduced by setting the orientations of both stations perpendicular. This consideration was applied at stations S2 and S3.

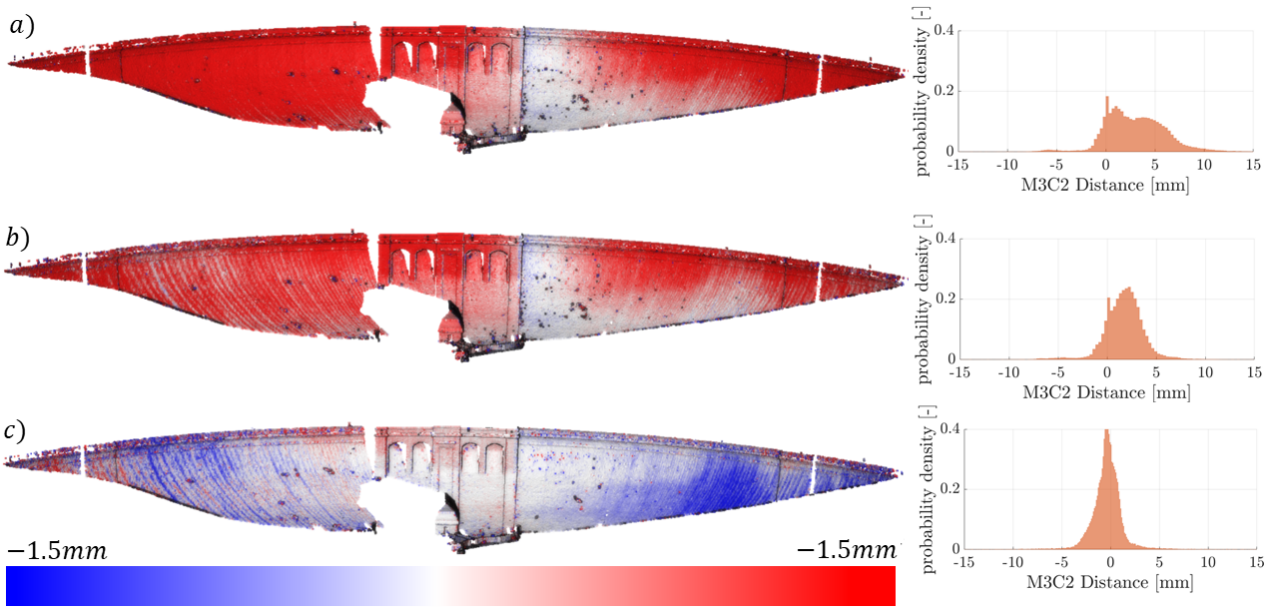

Figure 2. M3C2 distances and their distributions of front and back face measurement for a) uncalibrated point cloud, b) after applying CPs estimated using Two-Face Method and c) after applying CPs estimated using combined Two-Face and Network Method.

4 Calibration Results

In this chapter we present the impact of TLS calibration on the point cloud.

4.1 Uncalibrated Point Cloud

For evaluation and visualization, we use the point cloud captured from station S1. A point cloud comparison using the M3C2 comparison between front and back face highlights issues caused by insufficient calibration, thereby indicating the effectiveness of the calibration process. This is because some calibration parameters are sensitive to two faces (see table 1). To properly assess calibration through point cloud comparisons, scans from different stations would be necessary. However, this would primarily reveal effects from the registration rather than from calibration. The left part of figure 2a) presents the performed point cloud comparison, where blue indicates negative deviations and red represents positive deviations. The right part of the figure displays the histogram of the M3C2 distances.

The visualization reveals distinct systematic differences between front and back face. The magnitude of systematic deviations are comparable low the change of faces but become more prominent towards the edges of the dam. The histogram of M3C2 distances confirms these systematics. The distribution function is noticeably skewed in the positive direction. Table 3 shows the mean value and the RMS (root mean square error) of the M3C2 distances.

4.2 Calibration using Two-Face Method

As shown in Figure 1, the captured data consists of many vegetation, which can move between front and back face measurement due to wind. To avoid effects, we focused solely on the dam for in-situ calibration. As explained in section 2.4, intensity images, range images of both faces were generated and were detected. The resulting dataset consists of intensity and range images with a resolution of 7883 x 20269 pix. In front face, 9095 keypoints were identified, while back face contains 9003 keypoints. With 42% we can match 3886 keypoints in two faces which can be used as identical points. Figure 3 presents a section of the intensity image, highlighting the keypoints detected and successfully matched in front and back faces. Keypoints are evenly distributed across the entire dam, with a higher concentration of matches near the scanner. However, a sufficient number of matches are also present throughout the dam, including areas at the dam's crown. The spherical coordinates derived from the intensity and range image (see section 2.4)

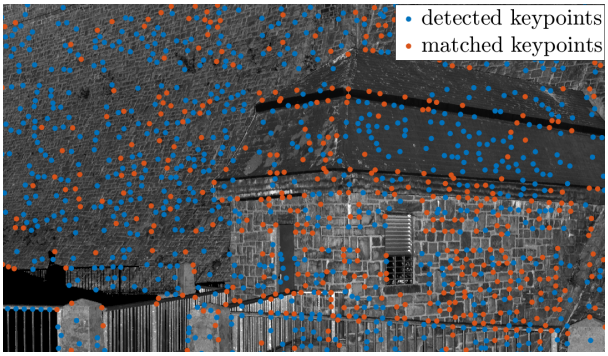

Figure 3. Section of intensity image with detected and matched keypoints using front face scan.

Table 2. Estimated CPs by using Two-Face Method.

CP	$\hat{p}$	$\sigma_{\hat{p}}$	$max(\rho_{\hat{p}})$	with
x_{1z}	5.92 *mm*	0.19 *mm*	0.44	x_{5z7}
x_2	0.04 *mm*	0.06 *mm*	0.64	x_4
x_3	0.66 *mm*	0.04 *mm*	0.95	x_6
x_4	$-0.53''$	$2.7''$	0.99	x_{5z7}
x_{5z7}	$-1.08''$	$2.77''$	0.99	x_4

are used to determine the corresponding CPs as described in section 2.2.
Since the Two-Face Method relies solely on data measured from a single station in front and back face, only CPs that are sensitive to two faces can be determined (indicated by * in table 1). Additionally, the dam presents a challenging measurement geometry, as no keypoints have vertical angles $< 59^{\circ}$ which has an unfavorable effect on the determinability of the parameters. Due to the proximity of the station to the dam, many measurements exhibit high incidence angles, introducing additional systematic effects unrelated to geometric misalignments. As a result, only the CPs x_{1z}, x_2, x_3, x_4, x_{5z}, x_6 and x_7 can be determined. The CPs x_{5z} and x_7 have the same functional impact on the horizontal angle (see equation 3), making them indistinguishable in calibration. They are therefore combined into a new parameter $x_{5z7} = x_{5z} - x_7$. For every estimated parameter the estimated value $\hat{p}$ and the corresponding standard deviation $\sigma_{\hat{p}}$ as well as maximal correlation coefficient $max(\rho_{\hat{p}})$ and the maximal CP is shown. The estimated CPs are applied to the point cloud, and M3C2 differences are calculated, just as in the uncalibrated case. The left part of figure 2b) visualizes these differences, while the histogram on the right presents the computed differences for the calibrated point cloud.
Compared to the uncalibrated point cloud, the distribution of differences becomes narrower and more closely to a normal distribution. Across the entire dam, the overall magnitude of deviation between the two faces is reduced; however, noticeable systematic effects are visible near the edges. Deviations in both faces remain predominantly positive. As shown in Table 3, the mean value moves closer to zero, and the RMS is also reduced.

Table 3. Statistical properties of the M3C2 differences.

method	mean [mm]	RMS [mm]
uncalibrated	2.9	4.3
Two-Face Method	1.7	2.8
Two-Face + Network Method	−0.36	2.0

4.3 Calibration using combined Two-Face and Network Method

We also estimate CPs by using the combined Two-Face and Network Method. For the Two-Face Method part we using the same data as in 2.2, for the Network Method part, front and back face scans of targets T1-T9 from stations S3 and S4 are used. Janßen et al. (2019) analyzed empirically the stochastic model of the BOTA 8 targets, which is applied for calibration in this study. This method allows the determination of all CPs in table 1. As in the Two-Face Method, the CPs $x_{5}z$ and x_7 which influences the horizontal angle are combined to $x_{5z7} = x_{5z} - x_7$. Similarly, for vertical angle measurement, parameters x_{5z} and x_{9z}, as well as x_{5n} and x_{9n}, exhibit the same functional impact. By combining these pairs, the new parameters $x_{5z9z} = x_{5z} + x_{9z}$ and $x_{5n9n} = x_{5n} + x_{9n}$ are introduced. As a result, the total number of parameters to be determined is reduced from 18 to 16. Estimated CPs including standard deviations and correlations are presented in table 4. Figure 2c) illustrates computed M3C2 differences after applying CPs to the point cloud. The overall magnitude of the M3C2 deviations across the dam is significantly reduced compared to the uncalibrated case. Table 3 shows, that mean M3C2 differences and RMSs are also reduced compared to the Two-Face Method. Systematic deviations are

Table 4. Estimated CPs by using combined Network and Two-Face Method.

CP	$\hat{p}$	$\sigma_{\hat{p}}$	$max(\rho_{\hat{p}})$	**with**
x_{1z}	$-0.84\ mm$	$0.07\ mm$	0.37	x_{12a}
x_2	$0.07\ mm$	$0.01\ mm$	0.16	x_{12b}
x_3	$0.01\ mm$	$0.01\ mm$	0.04	x_2
x_4	$-0.51''$	$0.12''$	0.52	x_{8y}
x_6	$-5.43''$	$0.08''$	0.54	x_{11a}
x_{5z7}	$-12.15''$	$0.6''$	0.80	x_{11b}
x_{1n}	$-0.41\ mm$	$0.01\ mm$	0.74	x_{5z9z}
x_{8x}	$12.11''$	$0.08''$	0.70	x_{12a}
x_{8y}	$-10.05''$	$0.15''$	0.52	x_4
x_{5n9n}	$11.7''$	$0.28''$	0.36	x_6
x_{5z9z}	$26.29''$	$0.52''$	0.74	x_{1n}
x_{10}	$0.36\ mm$	$0.03\ mm$	0.44	x_{1n}
x_{11a}	$4.13''$	$0.89''$	0.54	x_6
x_{11b}	$10.92''$	$0.87''$	0.80	x_{5z7}
x_{12a}	$-3.3''$	$0.15''$	0.70	x_{8x}
x_{12b}	$17.91''$	$2.07''$	0.44	x_{11a}

still present but are significantly reduced through calibration. Notably, the deviations shift towards zeros. In contrast to the Two-Face Method, more deviations now are negative. Unlike the left (negative) side of the histogram, the distribution on the right (positive) side now closely resembles a normal distribution.

5 Discussion

Both calibration methods effectively reduce systematic effects. This can be verified by a direct two-face M3C2 point cloud comparison. Calibration minimizes the impact of many systemic influences to a level below the expected random measurement noise, despite measuring distances of 100 m in some cases.

However, systematic deviations cannot be entirely eliminated. Even after calibration, noticeable effects remain at the edges of the dam, likely caused by high incidence angles rather than internal scanner misalignments, making them irreducible with the presented methods. The same applies to points near the zenith. If all systematic influences were completely removed, the M3C2 distances would follow a normal distribution with a mean of zero. While calibration brings the distribution closer to a normal distribution, it does not fully achieve it. Due to remaining systematic effects, a perfectly normal distribution of differences cannot be expected.

Since the Two-Face Method does not estimate all parameters, the overlapping parameters between both methods show discrepancies. Notably, in the Two-Face Method, parameters x_2, x_4 and x_{5z7} exhibit particularly large standard deviations, often comparable in magnitude to the parameters themselves. Additionally, these parameters show strong correlations with others. In contrast, when using all parameters in the combined approach, both standard deviations and correlations are reduced.

Both approaches enhance the quality of the point cloud. While the Two-Face Method offers less potential for improvement, it requires no additional measuring equipment. If artificial targets are already being used for registration, the combined approach yields even greater improvements.

6 Conclusion and Outlook

We introduced Two-Face and combined Two-Face and Network Method to estimate calibration parameters. While the combined Two-Face and Network Method allows the determination of all calibration parameters, the Two-Face Method alone provides only a subset. Nevertheless, both approaches significantly reduce systematic effects caused by internal scanner misalignments. As self-calibration methods, they require no additional measuring equipment beyond the existing setup, making them easy to integrate into the measurement process.

The data shows remaining systematic effects. Certain calibration parameters exhibit high standard deviations and correlations. These issues arise from measurement configurations that cannot be adjusted in-situ. A potential solution would be performing a-priori calibration immediately before measurement using optimized calibration fields.

In the combined method, artificial targets are used to ensure that identical points are visible from multiple stations. To increase the number of identical points, keypoints could be incorporated. However, to mitigate challenges arising from varying viewpoints during keypoint extraction and matching, it would likely be necessary to use 3D keypoints instead of the 2D keypoints applied in this study.

The M3C2 point cloud comparison of front and back face assesses only systematic effects that are sensitive to two faces. To evaluate all effects

comprehensively, future studies could incorporate length normals into the environment. These would enable the assessment of all calibration parameters.

Acknowledgements

This research was funded by German Research Foundation (DFG) under grant number 490989047, "Research Unit 5455 Deformation analysis based on terrestrial laser scanner measurements (TLS-Defo)".

References

Förstner, W. and Gülch, E. (1987). A fast operator for detection and precise location of distinct points, corners and centres of circular features. In *Proc. ISPRS intercommission conference on fast processing of photogrammetric data*, volume 6, pages 281–305. Interlaken.

Janßen, J., Medic, T., Kuhlmann, H., and Holst, C. (2019). Decreasing the uncertainty of the target center estimation at terrestrial laser scanning by choosing the best algorithm and by improving the target design. *Remote Sensing*, 11:845.

Koch, K.-R. (2013). *Parameter estimation and hypothesis testing in linear models*. Springer Science & Business Media.

Leutenegger, S., Chli, M., and Siegwart, R. Y. (2011). Brisk: Binary robust invariant scalable keypoints. In *2011 International conference on computer vision*, pages 2548–2555. Ieee.

Lichti, D. D. (2007). Error modelling, calibration and analysis of an am–cw terrestrial laser scanner system. *ISPRS Journal of Photogrammetry and Remote Sensing*, 61(5):307–324.

Lichti, D. D. (2010). Terrestrial laser scanner self-calibration: Correlation sources and their mitigation. *ISPRS Journal of Photogrammetry and Remote Sensing*, 65(1):93–102.

Lichti, D. D., Pexman, K., and Tredoux, W. (2021). New method for first-order network design applied to tls self-calibration networks. *ISPRS Journal of Photogrammetry and Remote Sensing*, 177:306–318.

Medić, T., Kuhlmann, H., and Holst, C. (2019a). Automatic in-situ self-calibration of a panoramic tls from a single station using 2d keypoints. *ISPRS Annals of the Photogrammetry, Remote Sensing and Spatial Information Sciences*, 4:413–420.

Medić, T., Kuhlmann, H., and Holst, C. (2019b). Designing and evaluating a user-oriented calibration field for the target-based self-calibration of panoramic terrestrial laser scanners. *Remote Sensing*, 12(1):15.

Medić, T., Kuhlmann, H., and Holst, C. (2021). A priori vs. in-situ terrestrial laser scanner calibration in the context of the instability of calibration parameters. In *Contributions to International Conferences on Engineering Surveying: 8th INGEO International Conference on Engineering Surveying and 4th SIG Symposium on Engineering Geodesy*, pages 128–141. Springer.

Muralikrishnan, B. (2021). Performance evaluation of terrestrial laser scanners—a review. *Measurement Science and Technology*, 32(7):072001.

Reshetyuk, Y. (2009). *Self-calibration and direct georeferencing in terrestrial laser scanning*. PhD thesis, KTH.

Schwarz, W. (2018). *Ingenieurgeodäsie: Handbuch der Geodäsie, herausgegeben von Willi Freeden und Reiner Rummel*. Springer.

Wang, L., Muralikrishnan, B., Rachakonda, P., and Sawyer, D. (2017). Determining geometric error model parameters of a terrestrial laser scanner through two-face, length-consistency, and network methods. *Measurement Science and Technology*, 28(6):065016.